Crystallization of icosahedral $Al_{86}Mn_{14}$

K. F. Kelton and J. C. Holzer
Department of Physics, Washington University, St. Louis, Missouri 63130
(Received 27 April 1987; revised manuscript received 21 September 1987)

Isothermal measurements of the crystallization kinetics of icosahedral $Al_{86}Mn_{14}$ were made by differential scanning calorimetry and electrical resistivity in the temperature range 593–723 K. Transmission electron microscopy investigations of as-quenched samples showed that the icosahedral phase (*i* phase) occurs as dendritic nodules separated by α-Al. On crystallization, Al_6Mn nucleates at the *i*-phase boundary and grows into the *i* phase, while consuming the α-Al. An effective-medium theory is used to relate resistance changes to the volume fraction transformed. A Johnson-Mehl-Avrami analysis for the kinetics of transformation indicates continuous nucleation with diffusion-limited growth. Nonisothermal differential scanning calorimetry measurements were made and analyzed using a numerical model that assumes simultaneous nucleation and growth. Crude estimates are given for the diffusion coefficient for growth of the crystal phase in the *i* phase and a lower bound for the *i*-phase Al_6Mn interfacial energy.

I. INTRODUCTION

It is generally accepted that the discovery by Shechtman *et al.*[1] of a fivefold phase in rapidly quenched $Al_{86}Mn_{14}$ is the first evidence for a new condensed-matter phase with extended icosahedral orientational symmetry. This symmetry is incompatible with long-range, periodic translational order; however, attempts to model this structure as a multiply twinned, complex crystal phase with a large unit cell[2,3] have failed to satisfactorily fit the x-ray diffraction or transmission electron microscopy data.[4]

With the exception of Al_6Li_3Cu,[5,6] the icosahedral phase is a metastable phase that is obtained by kinetically inhibiting the development of the stable crystalline phase. It is, therefore, important to determine the metastability of the icosahedral phase (*i* phase) by measuring the thermodynamic differences between this phase and the competing crystalline phases and the kinetics of transformation to the stable phases. Some measurements of the heat of transformation on crystallization of the icosahedral phase have been reported.[7–9] Several structural studies of the crystallization of the *i* phase also exist.[10–12] There are, however, no detailed investigations of the transformation kinetics using several complementary techniques on the same sample.

We present detailed measurements of the kinetics of crystallization for rapidly quenched $Al_{86}Mn_{14}$ over a wide temperature range, obtained by measuring the rate of heat evolution with differential scanning calorimetry (DSC) and changes in the electrical resistance. The crystallization products and mechanism are observed directly by transmission electron microscopy (TEM).

To determine the temperature dependence of the transformation coefficients, we have developed a technique for quantitatively analyzing the nonisothermal DSC data. The kinetic parameters obtained from this analysis agree with those obtained from a standard analysis of the isothermal DSC and the electrical resistance measurements. From this analysis, we present (1) the first estimates of the nucleation rate of the crystal from the *i* phase, (2) the diffusion coefficient for growth of the crystal phase in the *i* phase, and (3) a lower bound estimate for the crystal-icosahedral interfacial free energy.

II. EXPERIMENT

Alloys of the appropriate composition were first prepared by induction melting in a fused silica crucible that was partially backfilled with argon. These were subsequently quenched in a helium atmosphere onto a rotating copper disk whose surface velocity was maintained at approximately 30 m/sec. The ribbons were continuous for several feet with an average cross section of 1–2 mm by 20–30 μm.

Samples for transmission electron microscopy investigations were prepared by ion beam milling from both sides in a liquid-nitrogen-cooled sample stage. There was no difference between samples prepared by this method and those prepared by chemical jet thinning in an electrolyte of 1.5 vol % HNO_3, 5 vol % $HClO_4$, and methanol at -30 °C, indicating the absence of significant milling-induced sample damage. A JEOL 2000FX electron microscope was used to obtain the electron diffraction patterns and the microstructures of the as-quenched and transformed material.

The heat of transformation was measured isothermally and as a function of scan rate in a nitrogen atmosphere using a Perkin-Elmer model 7 differential scanning calorimeter, graphite and stainless-steel sample pans were used to avoid sample alloying with the pans. Temperature shifts in the differential scanning calorimeter during the scans due to thermal transients were determined by measuring the Curie temperature of Ni, which is independent of scan rate.

In situ four-probe measurements of the changes in the sample resistance were made using a computer-controlled dc bridge. Thermocouple effects were removed by

averaging the measurements for positive and negative applied voltages. The absolute stability of the bridge was better than one part in 10^4 over the course of the experiment.

Samples that were approximately 3 cm in length were placed in a ceramic holder constructed of Macor®; the holder was held in a copper shroud to ensure thermal equilibrium. Electrical contact to the sample was mechanically made with four small tungsten pins. A thermocouple was held in contact with the sample by a fifth tungsten pin.

The sample holder and shroud were initially seated in a water-cooled cold block. The chamber was evacuated and backfilled to a slight overpressure with 99.998% pure argon gas that was further purified by passing it over calcium chips held at 523 K. After the furnace was brought to the annealing temperature, the sample was loaded into the furnace with a vacuum feedthrough. The temperature measured at the sample reached the annealing temperature in 2–3 min with no measurable overshoot. The sample temperature was stable to within ±0.5 K over the period of the anneal. A detailed discussion of the apparatus is presented elsewhere.[13]

III. RESULTS

A. Transmission electron microscopy

The *i* phase in the as-quenched samples has the usual dendritic morphology with nodules of *i* phase separated by α-Al. TEM diffraction of the nodules for different sample orientations confirmed the icosahedral point group symmetry, $m\,\bar{3}\,\bar{5}$. These results are reported elsewhere.[7] The appearance of the nodules was mottled, which may indicate quenched-in strain or chemical inhomogeneities.

Short anneals above 600 K caused a decrease in the electrical resistivity (Sec. III B), but x-ray diffraction and TEM studies showed no evidence for crystallization of the *i* phase. The appearance of the nodules after this treatment was more uniform, which suggests that stress relaxation may occur prior to crystallization. This is probably accompanied by phase separation in the α-Al; this is discussed in more detail in Sec. III B. Annealing for longer times completely transforms the *i* phase to crystalline Al_6Mn.

Figure 1 shows a bright and dark field image of a partially transformed nodule from an approximately 30% crystallized sample. Nucleation occurs preferentially at the phase boundary between the *i* phase and the α-Al, however there is no evidence of saturation of the phase boundary. These observations agree with earlier studies by Urban *et al.*[10] The degree of transformation was different for different nodules. This may be due to a variable number of active nucleation sites or a statistical fluctuation in the nucleation rate because of the small nodule size. Analytical microscopy measurements of Kimura *et al.*[14] suggest that the stoichiometry of the *i* phase is near Al_4Mn; excess aluminum from the α phase, therefore, must be consumed to form crystalline Al_6Mn.

X-ray diffraction studies of the as-quenched samples showed peaks due to α-Al and the *i* phase. After complete transformation, lines corresponding to Al_6Mn and α-Al were noted.

B. Electrical resistivity

The extrapolated residual electrical resistivity of the as-quenched sample is 71 ± 10 $\mu\Omega$ cm. The temperature coefficient is $(2.3\pm0.05)\times10^{-4}$ K^{-1}. The extrapolated residual resistivity of the transformed sample is lower by a factor of 35 and the temperature coefficient of resistivity, 0.05 K^{-1}, is greater by a factor of 50. The spread in temperature coefficients obtained from different transformed samples is less than 5%.

Figure 2 shows the change in the sample resistance, normalized to the initial value at room temperature of the as-quenched sample, as the temperature is cycled between 300 and 900 K at 5 K/min. Two distinct stages in the transformation are noticed. In the first stage the resistance decreases by approximately 20%, going through a minimum at 685 K. Decreasing the sample

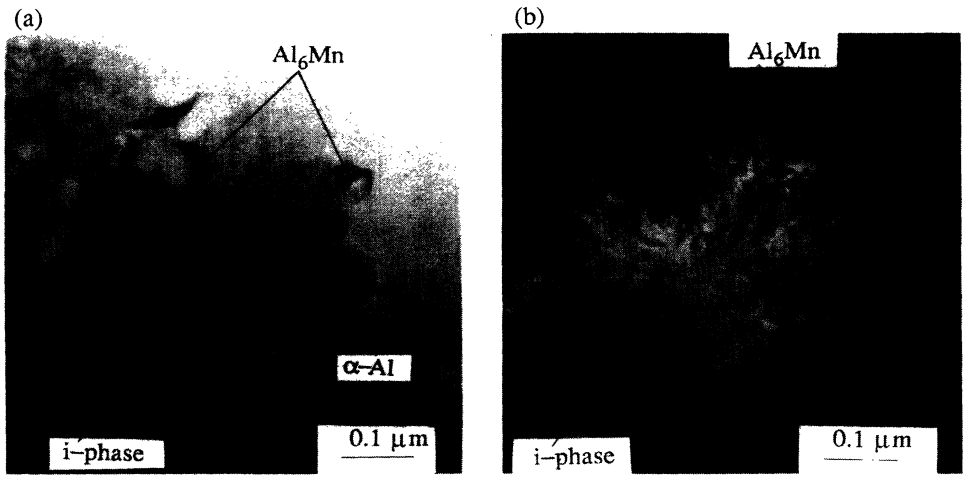

FIG. 1. (a) Bright field (b) and dark field TEM images of a partially transformed *i*-phase nodule. The α-Al, *i* phase, and Al_6Mn are indicated.

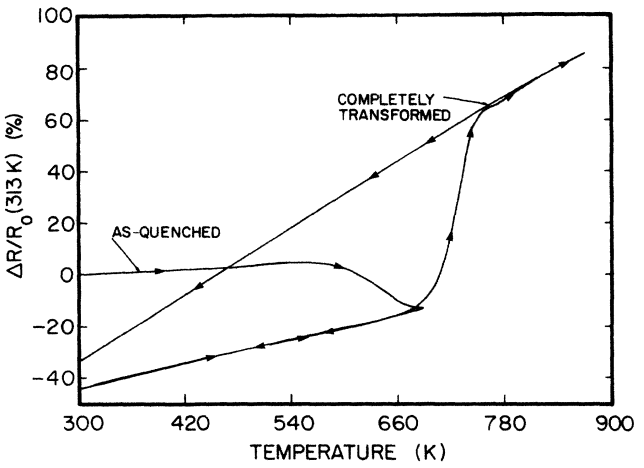

FIG. 2. The temperature variation of the resistance, normalized to the room-temperature resistance, for as-quenched $Al_{86}Mn_{14}$ as the temperature is scanned at 5 K/min.

temperature at that point shows that the temperature coefficient of resistivity has increased to $(2.3\pm0.1)\times10^{-3}$ K^{-1}. On reheating, the resistance increases above the temperature-induced changes by approximately 80% over the temperature range of 685–760 K. On cooling, the temperature coefficient is that of the fully transformed sample, 0.05 K^{-1}. This initial decrease of the resistance followed by an increase was also observed by Pavuna *et al.*[15]

The change in the sample resistance, normalized to the initial resistance at the annealing temperature, is plotted as a function of annealing time for all annealing temperatures in Fig. 3. As in the nonisothermal case, two regions of behavior are observed. For short annealing times, the resistivity decreases by approximately 25%. X-ray diffraction and TEM studies of samples annealed to the minimum in the resistance change, however, give no evidence of a phase transformation. The resistance increases by approximately 40–50% during the second stage of the transformation. The temperature coefficient of resistivity also increases from 2.3×10^{-3} K^{-1} at the resistance minimum to 0.05 K^{-1} for the fully transformed samples.

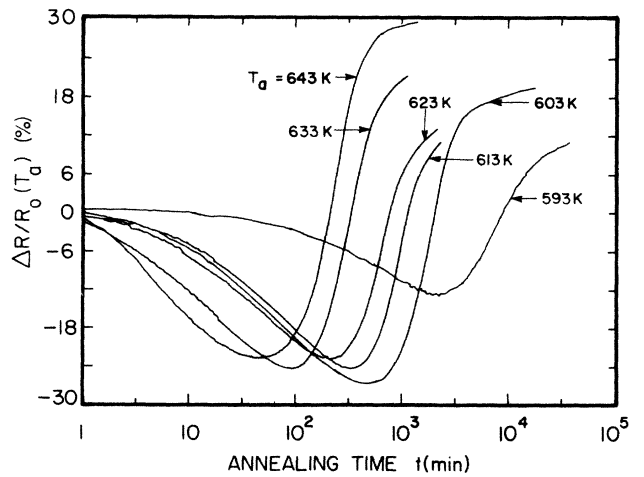

FIG. 3. Relative change in resistance of as-quenched $Al_{86}Mn_{14}$ ribbons at several temperatures.

The magnitude of the resistance change is different for different annealing temperatures; it often increases with increasing annealing temperatures. This is due in part to the different temperature coefficients of the various phases arising during the transformation. The additional sample variations probably arise from different initial morphologies of the highly conductive α phase. Since kinetic information is extracted from the time dependence of the fractional change, these variations are not expected to seriously affect the analysis.

The initial decrease in resistance presumably arises from a precipitation reaction in the α-Al. X-ray dispersive measurements of Krishnan *et al.*[16] indicate that the α phase is a solid solution of Al and 4% Mn. This is a metastable configuration quenched from high temperatures and is well above the equilibrium solubility limit of Mn in Al at the annealing temperatures. The equilibrium phase diagram indicates that phase separation into α-Al and Al_6Mn should occur. Since the *i* phase is present, however, removal of the excess Mn may also occur by further growth of that phase; the exponential resistance decrease during this transformation suggests growth without nucleation. By either mechanism, Mn will be removed from solution. The addition of small amounts of Mn to Al causes a large increase in the electrical resistivity and a decrease in the temperature coefficient.[17] Decreasing the Mn in solution will therefore decrease the resistance and increase the temperature coefficient in agreement with observation. X-ray and TEM measurements cannot detect the 2% maximum increase in the amount of *i* phase or Al_6Mn that results from this phase separation.

TEM and x-ray diffraction measurements confirm that the resistance increase in the second stage is due to the crystallization of the *i* phase and a simultaneous consumption of the α-Al. These resistance changes are analyzed in Sec. IV B to obtain kinetic information on the crystallization of the *i* phase.

C. Differential scanning calorimetry

The transformation was investigated using isothermal and nonisothermal DSC. The heat of crystallization is 13.1 ± 0.6 cal/g or, assuming an average atom of Al_4Mn, 0.58 ± 0.03 kcal/g-at. Figure 4 shows the DSC measurements of the crystallization, normalized to the peak value, for scan rates from 2.5 to 80 K/min. The fits are to a model developed in the next section. Isothermal DSC measurements of the heat evolved on transformation were also used to determine the mode and kinetics of the reaction. Those results are presented and analyzed with the isothermal electrical resistivity results in Sec. IV C.

IV. DISCUSSION

A. Transformation theory

The Johnson-Mehl-Avrami (JMA) theory[18,19] describes the time evolution of the volume fraction transformed, *x*,

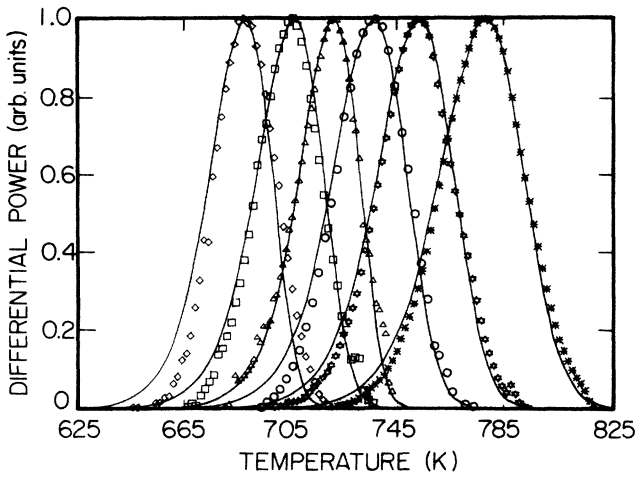

FIG. 4. DSC traces for as-quenched $Al_{86}Mn_{14}$ for various scan rates: ◇, 2.5 K/min; □, 5 K/min; △, 10 K/min; ○, 20 K/min; ✡, 40 K/min; *, 80 K/min. The traces are normalized to the peak heights. The fits are to a model that assumes nucleation and growth.

in terms of the nucleation rate per unit volume, I_v, and the crystal growth velocity u, taking into account possible overlap of the transformed regions. Assuming that the nucleation rate and growth velocity are independent of time (t),

$$x(t)=1-\exp(-\alpha' I_v u^m t^n) , \tag{1}$$

where $n=m+1$. Here, α' is a geometrical factor that depends on the shape of the transforming phase and m is an integer or half-integer that depends on the growth mechanism and the dimensionality of the crystal.

It is often assumed that the growth velocity and the nucleation rates have an Arrhenius temperature dependence. This leads to the more familiar form for the JMA equation,

$$x(t)=1-\exp[-(kt)^n] , \tag{2}$$

where k is an overall transformation coefficient with an effective activation energy Q:

$$k=k_0\exp(-Q/k_B T) , \tag{3}$$

where k_0 is a temperature-independent constant, and k_B is Boltzmann's constant. Equation (2) may be written as

$$\ln\left[\ln\left[\frac{1}{1-x}\right]\right]\equiv\ln(\xi)=n\ln(k)+n\ln(t) . \tag{4}$$

By these assumptions, a plot (often referred to as an Avrami plot) of $\ln(\xi)$ versus $\ln(t)$ should yield a straight line with slope n, and intercept $n\ln(k)$.

B. Electrical resistivity

It is normally assumed that the resistivity change scales with the change in the volume fraction transformed. Analyzing the resistance data presented in Fig. 3 with this assumption, however, produced continuously curved Avrami plots whose interpretation was not consistent with the TEM and DSC measurements.

As discussed, the transformation does not occur randomly in space but nucleates preferentially on the boundary of the i phase. Further, the volume fraction of the highly conductive α-Al decreases as the transformation proceeds due to the different stoichiometry of the i phase and Al_6Mn. Clearly, changes in the resistivity will not depend linearly on the volume fraction transformed.

The resistivity changes are modeled by ellipsoids of revolution of the i phase and Al_6Mn that are embedded in the α-Al. Using an effective-medium theory,[20] the effective resistivity ρ_{eff} is

$$\begin{aligned}2\rho_{\text{eff}}=&\rho_i\left[1-\frac{f_\alpha}{X}\right]+\rho_\alpha\left[1-\frac{f_i}{X}\right]\\&+\left\{\left[\rho_i\left[1-\frac{f_\alpha}{X}\right]+\rho_\alpha\left[1-\frac{f_i}{X}\right]\right]^2\right.\\&\left.-4\rho_i\rho_\alpha\left[1-\frac{1}{X}\right]\right\}^{1/2} ,\end{aligned} \tag{5}$$

where ρ_i and f_i are the resistivity and volume fraction, respectively, of the mixture of the i phase and Al_6Mn, and ρ_α and f_α are the resistivity and volume fraction of the α phase. X is a measure of the eccentricity, ϵ, of the ellipsoids and is defined by

$$X=\frac{1-\epsilon^2}{\epsilon^3}\left[\tfrac{1}{2}\ln\left[\frac{1+\epsilon}{1-\epsilon}\right]-\epsilon\right] . \tag{6}$$

The value of X had no significant effect on the analysis; it was therefore set to $\frac{1}{3}$, the value for a sphere.

Two extreme cases were considered to estimate the effective resistivity of the icosahedral-crystal nodule, $\rho_i(t)$. In one case, $\rho_i(t)$ was calculated by assuming that a complete crystalline shell forms and grows into the i phase. For the other case, the crystal was assumed to nucleate and grow randomly in the icosahedral nodule. For small volume fractions, these models should differ in their predictions; for large fractions transformed, they should approach each other. Both models made similar predictions for the volume fraction transformed as a function of time. This suggests that the most significant effect on the electrical resistivity in the initial stages of the transformation is due to the decreasing volume fraction of the α-Al. Using Eq. (5), the residual resistivity of the icosahedral phase was estimated as 130 $\mu\Omega$ cm; the residual resistivity of Al_6Mn was 3.7 $\mu\Omega$ cm. Figure 5 shows the resistivity as a function of the volume fraction transformed, x, calculated from the effective-medium model using these values for ρ and assuming a linear relation between ρ_{eff} and x. The linear approximation is in error for this case.

An Avrami plot of the volume fraction transformed, computed from the resistance data in Fig. 3 by using the effective-medium model, is shown in Fig. 6. Straight lines are obtained with slope $n=2.2\pm0.2$, suggesting a diffusion-controlled reaction with a slowly decreasing nucleation rate. This interpretation is in agreement with the TEM results.

The kinetic coefficients k obtained from the intercepts of these fits are plotted in Fig. 9. Assuming Eq. (3), we

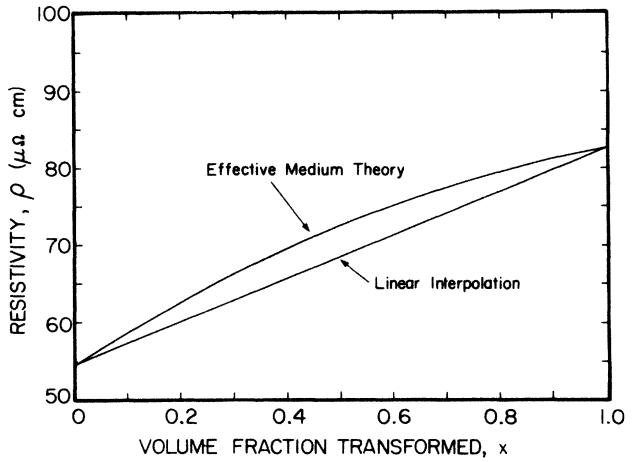

FIG. 5. Sample calculations of the resistivity as a function of volume fraction transformed for the two models discussed.

obtain an activation energy $Q=2.4$ eV from the resistance measurements. The fit is to a model described in Sec. IV D.

C. Isothermal DSC

DSC isothermal measurements were made for annealing temperatures 683–723 K. The heat released is assumed to scale linearly with $x(t)$. To remove thermal transients, the samples were first held for 2–3 min at 30 K below the annealing temperature. The sample temperature was then increased to the annealing temperature at 40 K/min. An Avrami plot of the volume fraction transformed is shown in Fig. 7. The average slope gave an Avrami exponent, $n=1.6\pm0.4$, which is lower than the value of 2.2 obtained from the electrical resistivity measurements. This difference probably arises from partial saturation of the phase boundary nucleation sites during the short preanneal required to equilibrate the DSC. The kinetic coefficients obtained from the intercepts of these curves are plotted in Fig. 9.

More scatter is observed in the DSC data than in the electrical resistivity data. This may be due in part to poor thermal equilibration for the large sample sizes required (>20 mg), or it may reflect differences in samples from different quenches. With the exception of the measurements at 593 and 603 K, all of the resistance samples came from the same quench.

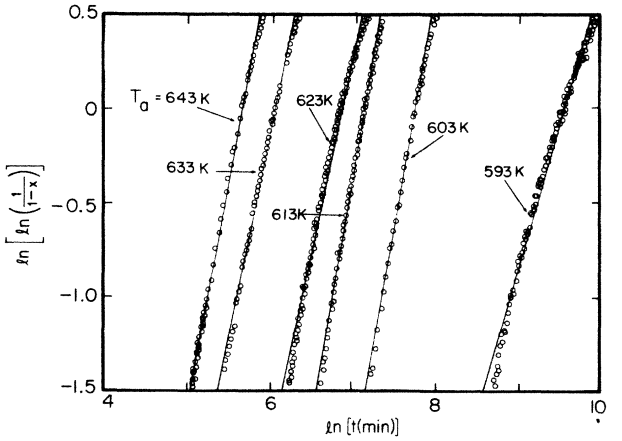

FIG. 6. Avrami plots constructed from the changes in resistance for various temperatures, T_a.

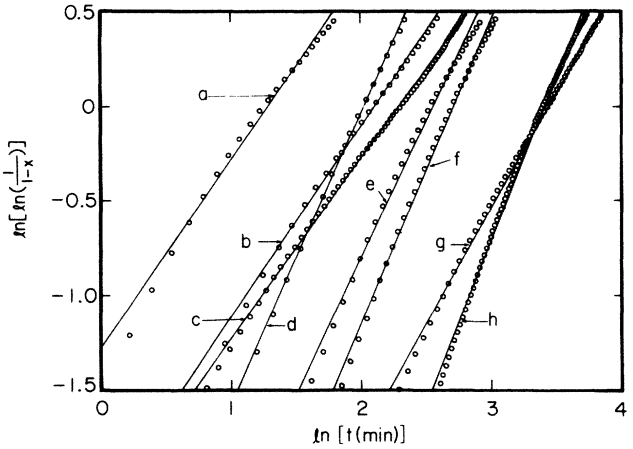

FIG. 7. Avrami plots constructed from the DSC isothermal measurements of the heat evolution for various temperatures and sample quenches. Curve a, quench 1, $T_a=723$ K; curve b, quench 1, $T_a=713$ K; curve c, quench 1, $T_a=703$ K; curve d, quench 2, $T_a=693$ K; curve e, quench 3, $T_a=693$ K; curve f, quench 2, $T_a=683$ K; curve g, quench 3, $T_a=683$ K; and curve h, quench 3, $T_a=673$ K.

D. Nonisothermal DSC

For nonisothermal transformations in DSC, the peak position depends on the scan rate. Several mathematical schemes for analyzing these peak shifts have been proposed. All of those treatments are based on the JMA theory and make various approximations to yield a tractable analytical expression. These techniques have recently been reviewed by Yinnon and Uhlmann.[21] The Kissinger method[22,23] is the most frequently used. It relates the heating rate (H), the effective activation energy of the transformation (Q), and the temperature of the maximum of the peak (T_p), as

$$\ln(H/T_p^2)=-(Q/k_BT_p)+C\ , \tag{7}$$

where C is a constant. Figure 8 shows the results of a Kissinger analysis of the DSC scans taken at 2.5, 5, 10, 20, 40, and 80 K/min. A linear plot is obtained with an activation energy of 1.65 eV, which is lower than the 2.4-eV value obtained from the resistance isothermal measurements.

The most significant error shared by all of the existing analytical expressions is the assumption of an Arrhenius temperature dependence for the nucleation rate. We present results of an analysis based on a more rigorous model of the transformation that includes a realistic temperature dependence for the nucleation rate. A brief description of the model is presented here. It will be discussed in greater detail and compared with existing analytical expressions in a future publication.

Following the TEM observation, we assume that the crystal phase nucleates at the α,i-phase boundary and

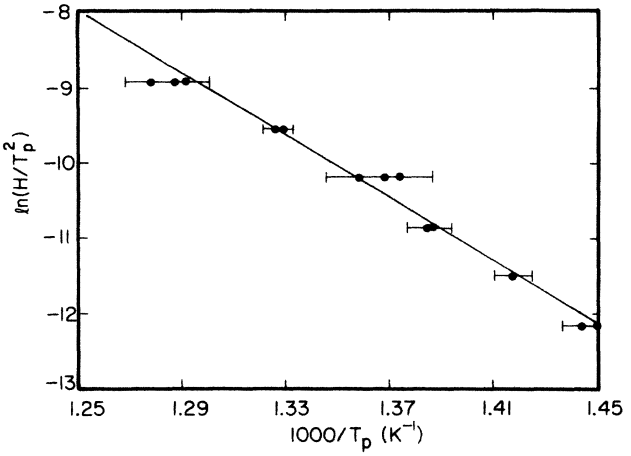

FIG. 8. Kissinger analysis of DSC scans for the crystallization of as-quenched $Al_{86}Mn_{14}$. H is the heating rate and T_p is the temperature of the peak maximum.

grows approximately hemispherically into the i phase. Using the classical expression for the steady-state, grain boundary nucleation rate per unit volume,[24,25]

$$ {}^{B}I_v = \frac{24A\,{}^{B}N_v n^{*(2/3)}}{\lambda^2}\left[\frac{\bar{v}\,|\,\Delta G_v\,|}{6\pi k_B T n^*}\right]^{1/2} \times D\exp\left[-\frac{16\pi}{3k_BT}\frac{\sigma^3}{\Delta G_v^2}S(\theta)\right], \tag{8} $$

where ${}^{B}N_v$ is the number of boundary atoms per unit volume, λ is the atomic jump distance, $\bar{v}$ is the atomic volume, D is an effective diffusion coefficient, ΔG_v is the volume free energy of the untransformed phase less that of the transformed phase, σ is the interfacial energy between the untransformed and transformed phases, and A is a constant of order unity that depends on the geometry of the developing nucleus. $S(\theta)$ is a function of the wetting angle for the crystalline phase at the phase boundary and is given by

$$ S(\theta)=(2+\cos\theta)(1-\cos\theta)^2/4\ . \tag{9} $$

The critical cluster size n^* is that cluster size above which it is energetically favorable to grow. The number of atoms in the critical cluster is given by

$$ n^* = B(\theta)\frac{32\pi}{3\bar{v}}\left[\frac{\sigma}{|\,\Delta G_v\,|}\right]^3, \tag{10} $$

where $B(\theta)$ is a weak function of θ of order 1; for spherical nucleation, $B(\theta)=1$, and for hemispherical nucleation, $B(\theta)=\frac{1}{2}$. The bulk free energy ΔG_v is calculated from the expression due to Turnbull,[26]

$$ \Delta G_v = \frac{\Delta H_f}{N_A\bar{v}T_0}(T-T_0)\ , \tag{11} $$

where ΔH_f is the measured heat of transformation, N_A is Avogadro's number, and T_0 is the temperature below which the crystal is stable. The accuracy of this analysis does not warrant the use of more refined estimates for ΔG_v. The atomic volume is estimated from the measured density[7] as 1.51×10^{-29} m^3. The activation energy for growth was taken to be 2.4 eV, in agreement with the activation energy for transformation at the lowest temperatures where the transformation is growth limited. Because the temperature range of the kinetic measurements is small, the analysis is not sensitive to the temperature dependence of σ. We therefore assume that σ is temperature independent.

For a diffusion-controlled transformation to phase β with hemispherical nucleation and growth, the volume fraction transformed as a function of time for isothermal annealing is approximately[27]

$$ x(t)=1-\exp\left[\frac{(c^\beta-c^\alpha)}{(c^m-c^\alpha)}\int_0^t(2\pi/3)(\alpha_3)^3D^{3/2}(t-\tau)^{3/2}\,{}^{B}I_v\,d\tau\right], \tag{12} $$

where c^β and c^α are the equilibrium concentrations of solute atoms in phase β and at the growing interface, respectively, and c^m is the mean concentration of the untransformed phase far from the interface; α_3 is a measure of the supersaturation. Assuming that ${}^{B}I_v$ and D are independent of time, using Eq. (11) to evaluate ΔG_v, and assuming an Arrhenius temperature dependence for the diffusion coefficient D, the effective transformation rate [defined in Eqs. (2) and (3)] is

$$ k=\frac{k_0}{T^{1/5}}\exp\left[-\frac{\Delta G_D}{k_BT}\right]\exp\left[-\frac{\alpha}{T(T-T_0)^2}\right], \tag{13} $$

where ΔG_D is the activation energy for diffusion. The constant, α is given by

$$ \alpha=\frac{32\pi S(\theta)\sigma^3T_0^2(N_A\bar{v})^2}{15k_B\Delta H_f^2} \tag{14} $$

and k_0 is given by

$$ k_0=D_0\left[\frac{32(6\pi^2\bar{v})^{1/3}\,{}^{B}N_v\,AB^{1/6}(\theta)}{15\lambda^2}\times\left[\frac{\sigma}{k_B}\right]^{1/2}\frac{(c^\beta-c^\alpha)}{(c^m-c^\alpha)}(\alpha_3)^3\right]^{1/2.5}, \tag{15} $$

where D_0 is the preexponential term for the diffusion coefficient.

The DSC scans were fit by extending Eqs. (2)–(4), using Eqs. (12)–(15), to nonisothermal conditions by approximating the continuous temperature change with a

series of short isothermal anneals. The transformation is assumed to be isokinetic, i.e., the rate of transformation is independent of the thermal history. The data were fitted by adjusting α, and k_0 for the least-squares error; the fits are shown in Fig. 4. The fit parameters were $\alpha=(4\pm2)\times10^8$ and $\ln k_0(\sec^{-1})=38.4\pm1.2$.

For this model, the nucleation is assumed to occur ramdomly in space and time, which is in contradiction with the TEM results. By extending Cahn's analysis of the transformation kinetics for grain boundary nucleation[28] to the present case with diffusion-limited growth, random nucleation is valid if $\chi\ (={}^BIDt^2)<1$, where ${}^BI$ is the grain boundary nucleation rate per unit area. An Avrami analysis will then yield $n\approx2.5$.

To further investigate this and the assumption of an isokinetic reaction, we simulated the transformation by following the development of individual crystallites in a 0.1-μm nodule of the i phase. Possible site saturation was included by appropriately decreasing the nucleation rate with the decreasing volume fraction of the untransformed boundary. The annealing time was divided into small time intervals and the nuclei that appear in each interval were calculated from Eq. (8). The growth on these nuclei was then computed for subsequent time intervals. This analysis gave $\alpha=(5\pm1.7)\times10^8$ with $\ln k_0(\sec^{-1})=37.5\pm1.2$, in agreement with the results from the simpler analysis based on the JMA equation.

Figure 9 shows the fit of the model to the isothermal resistivity and DSC data. The temperature dependence is fixed at the value determined from the nonisothermal fits, only the coefficient k_0 was allowed to vary. The fit gives $\ln k_0(\sec^{-1})=37.5\pm1.4$. The values for k_0 from the resistivity measurements and the nonisothermal calorimetry measurements are therefore in good agreement.

The reduction of the isothermal and nonisothermal data to the same master equation, the agreement with the results of a numerical simulation of the transformation, and the experimental support of the TEM data suggest

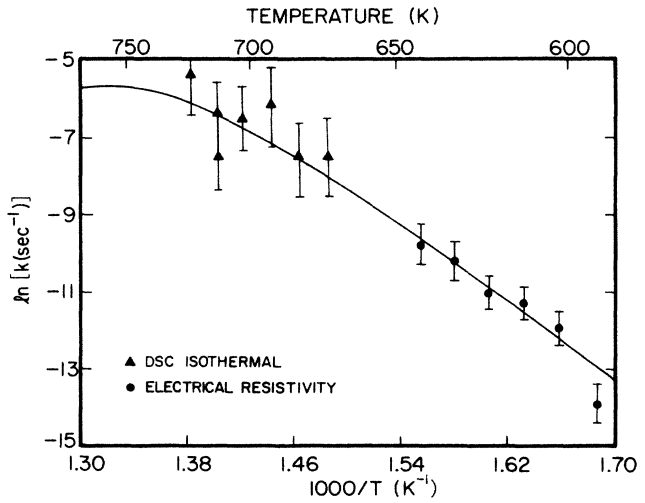

FIG. 9. Plot of ln$k$, the Avrami transformation coefficient, as a function of temperature for isothermal DSC and electrical resistivity measurements. The fit is to a model that assumes nucleation and growth.

that our model of the transformation is valid. With additional assumptions, crude estimates for the temperature dependence of the nucleation rate and the interfacial energy can be made. More direct methods, however, should be used to obtain quantitative information.

The peak nucleation temperature is estimated at 700 ± 10 K. The maximum nucleation rate is estimated using the numerical simulation of cluster growth as ${}^BI_v\approx10^{22\pm1}/\mathrm{m}^3\,\mathrm{sec}$. Assuming a 0.1-$\mu$m-diam nodule, this corresponds to 0.5–50 nucleation events per second, per nodule.

The peak transformation temperature is estimated as 750 ± 10 K. The DSC scans (Fig. 4) show a peak broadening for the faster scans with peak temperature greater than or approximately equal to 740 K, supporting our calculated maximum temperature.

The activation energy for growth (2.4 eV) should be equal to the activation energy for the diffusion of Al in Al_6Mn. The coefficient D_0 was estimated from the time for half crystallization for the low-temperature anneals, using the cluster simulation program. Estimating $1<\alpha_3^3<10$, $D_0\approx10^{-3}\ \mathrm{m}^2/\mathrm{sec}$.

It is difficult to obtain a reliable estimate of the interfacial energy from kinetic measurements. In this case, the nuclei are not observable due to the mottled appearance of the i phase; the contact angle is therefore unknown. The analysis is further complicated by the initial presence of two phases. All other things being equal, the nuclei interfaces will develop in the phase that minimizes the total interfacial energy. TEM measurements indicate that growth proceeds into the i phase but the behavior of the nuclei is unknown. Assuming, therefore, $\theta=90°$, and $T_0=931$ K, a lower bound estimate of the i-phase Al_6Mn interfacial energy ($\sigma_{i\text{-}c}$) can be set at 0.03 J/m^2. This is similar to the interfacial energy for crystalline metals and their liquids at the equilibrium melting temperature (for Al, $\sigma=0.09$ J/m^2 and for Mn, $\sigma=0.21$ J/m^2).[26] It is smaller than a typical orientationally averaged interfacial boundary energy between unlike crystalline phases.[29] The gram-atomic surface energy $\sigma^g_{i\text{-}c}$ is defined[26] as

$$\sigma^g_{i\text{-}c}=N_A\bar{v}^{2/3}\sigma_{i\text{-}c}\ . \tag{16}$$

Using the measured density,[7] $\sigma^g_{i\text{-}c}=1.1\times10^3$ J/g-at. Assuming that the interfacial energy scales with the heat of transformation, the ratio $\sigma^g_{i\text{-}c}/\Delta H_f$ is 0.45, which is also in reasonable agreement with the values for crystalline metals and their melts obtained from maximum undercooling data.[26] It is smaller than the more reliable value of 0.61 obtained for Hg from nucleation rate measurements.[30]

V. CONCLUSIONS

In this paper, measurements of the crystallization kinetics of quasicrystalline $Al_{86}Mn_{14}$ over a wide temperature range were presented and analyzed. The crystallization of the i phase was studied by isothermal measurements of changes in the electrical resistivity, by isothermal and nonisothermal measurements of the heat evolution in DSC, and by direct TEM observations.

TEM observations show that the i phase grows den-

dritically in the undercooled melt with dendrite arms approximately 0.1–0.3 μm in extent. The dendrites are separated by α-Al. Crystallization to Al_6Mn occurs by nucleation near the boundary between the *i* phase and the α-Al followed by growth into the icosahedral nodule with consumption of the α-Al.

The kinetics of crystallization for $593 \leq T \leq 653$ K were measured isothermally by electrical resistivity. The usual assumption that the resistivity scales linearly with the volume fraction transformed was shown to be in error. The effective-medium theory for the resistivity in an inhomogeneous medium was used to derive the volume fraction transformed as a function of time. An Avrami analysis gave an effective activation energy of 2.4 eV for the transformation and an Avrami exponent of 2.2, indicating nucleation with diffusion-controlled growth. Isothermal DSC measurements gave a lower Avrami exponent of 1.6. This is probably due to partial saturation of the nucleation sites.

The activation energy obtained from a Kissinger analysis of the DSC scans gave a smaller activation energy of 1.65 eV. This discrepancy was shown to be due to the assumption of an Arrhenius temperature dependence for the nucleation rate. Assuming a more realistic temperature dependence, a numerical method was presented that allows important quantitative information to be gained from nonisothermal DSC measurements. Using this method, we determined the nucleation rate and diffusion coefficient for the transformation; the peak in the nucleation rate occurs at 700±10 K and the maximum transformation rate occurs at 750±10 K. A lower bound estimate for the interfacial energy between the *i* phase and Al_6Mn is 0.03 J/m^2. The ratio of this value to the heat of transformation is 0.45 and is in reasonable agreement with the value for crystalline metals and their melts. These estimates of the interfacial energy of the *i* phase and the transformation kinetics provide important parameters that must be predicted by viable models of the *i* phase.

We are currently extending our numerical analysis by modeling the transformation behavior of a large ensemble of *i*-phase nodules. These results are planned to be discussed in a future publication.

ACKNOWLEDGMENTS

We thank F. Spaepen and Wataru Ohashi, Harvard University, for assistance with the x-ray diffraction measurements. We also thank Zheng Yu Li for helping with the sample production and J. W. Cahn, A. L. Greer, and A. E. Carlsson for useful comments. This research was supported by the National Science Foundation under Contract No. DMR-8604148.

[1]D. Shechtman, I. Blech, D. Gratias, and J. W. Cahn, Phys. Rev. Lett. **53**, 1951 (1984).
[2]L. Pauling, Nature (London) **317**, 512 (1985).
[3]L. Pauling, Phys. Rev. Lett. **58**, 365 (1987).
[4]J. W. Cahn, D. Gratias, and D. Schechtman, Nature (London) **319**, 102 (1986).
[5]M. D. Ball and D. J. Lloyd, Scr. Metall. **19**, 1065 (1985).
[6]M. A. Marcus and V. Elser, Philos. Mag. A **54**, L101 (1986).
[7]K. F. Kelton and T. W. Wu, Appl. Phys. Lett. **46**, 1059 (1985).
[8]H. S. Chen, C. H. Chen, A. Inoue, and J. T. Krause, Phys. Rev. B **32**, 1940 (1985).
[9]R. Lück, H. Haas, F. Sommer, and B. Predel, Scr. Metall. **20**, 677 (1986).
[10]K. Urban, N. Moser, and H. Kronmüller, Phys. Status Solidi **91**, 411 (1985).
[11]K. K. Fung and Y. Q. Zhou, Philos. Mag. **B54**, L27 (1986).
[12]R. Wang, J. Gui, S. Yao, Y. Cheng, G. Lu, and M. Huang, Philos. Mag. B **54**, L33 (1986).
[13]K. F. Kelton and J. C. Holzer, Rev. Sci. Instrum. (to be published).
[14]K. Kimura, T. Hashimoto, K. Suzuki, K. Nagayama, H. Ino, and S. Takeuchi, J. Phys. Soc. Jpn. **54**, 3217 (1985).
[15]D. Pavuna, C. Berger, F. Cyrot-Lackmann, P. Germi, and A. Pasturel, Solid State Commun. **59**, 11 (1986).
[16]K. M. Krishman, R. Gronsky, and L. E. Tanner, Scr. Metall. **20**, 239 (1986).
[17]D. Korn and G. Zibold, J. Phys. (Paris) **45**, 895 (1984).
[18]W. A. Johnson and R. F. Mehl, Trans. Am. Inst. Min. (Metall.) Eng. **135**, 416 (1939).
[19]M. Avrami, J. Chem. Phys. **7**, 1103 (1939).
[20]A. Davidson and M. Tinkham, Phys. Rev. B **13**, 3261 (1976).
[21]H. Yinnon and D. R. Uhlmann, J. Non-Cryst. Solids **54**, 253 (1983).
[22]H. E. Kissinger, J. Res. Nat. Bur. Stand. **57**, 217 (1956).
[23]D. W. Henderson, J. Non-Cryst. Solids **30**, 301 (1979).
[24]J. W. Christian, *The Theory of Transformations in Metals and Alloys* (Pergamon, Oxford, 1975), pp. 448–457.
[25]K. F. Kelton, A. L. Greer, and C. V. Thompson, J. Chem. Phys. **79**, 6261 (1983).
[26]D. Turnbull, J. Appl. Phys. **21**, 1022 (1950).
[27]J. W. Christian, *The Theory of Transformations in Metals and Alloys*, Ref. 24, pp. 534–542.
[28]J. W. Cahn, Acta Metall. **4**, 449 (1956).
[29]H. Gleiter and B. Chalmers, *Progress in Materials Science* (Pergamon, Oxford, 1972), Vol. 16, pp. 13–39.
[30]D. Turnbull, J. Chem. Phys. **20**, 411 (1952).

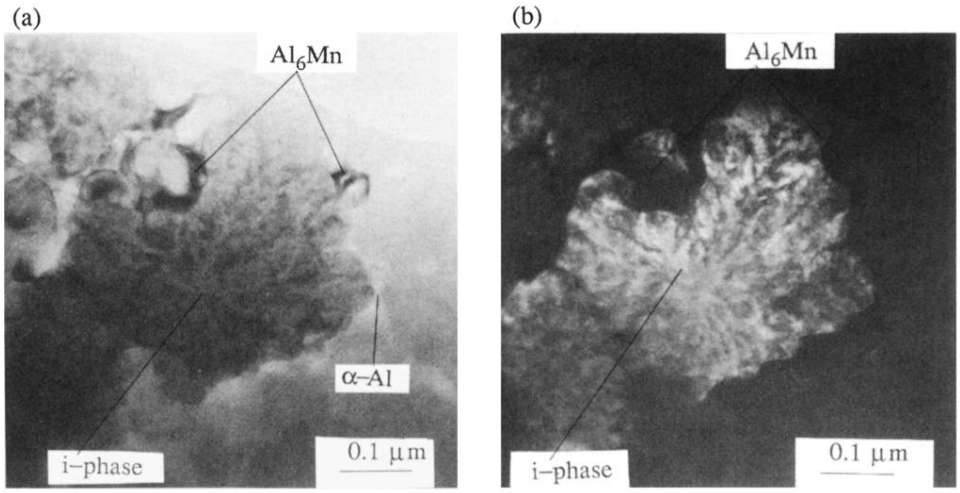

FIG. 1. (a) Bright field (b) and dark field TEM images of a partially transformed *i*-phase nodule. The α-Al, *i* phase, and Al_6Mn are indicated.